How temperature-induced depolymerization and plasticization affect the process of structural relaxation

Roman Svoboda[*1], Jana Machotová[2], Štěpán Podzimek[2], Pavla Honcová[3], Maria Chromčíková[4,5], Martina Nalezinková[6], Jan Loskot[7], Aleš Bezrouk[8], Daniel Jezbera[7]

[1]*Department of Physical Chemistry, Faculty of Chemical Technology, University of Pardubice, Studentská 573, 532 10 Pardubice, Czech Republic.*
[2]*Institute of Chemistry and Technology of Macromolecular Materials, Faculty of Chemical Technology, University of Pardubice, Studentská 573, 532 10 Pardubice, Czech Republic.*
[3]*Department of Inorganic Technology, Faculty of Chemical Technology, University of Pardubice, Studentská 573, 532 10 Pardubice, Czech Republic*
[4] *VILA – Joined Glass Centre of the IIC SAS, TnUAD, FChPT STU, Študentská 2, Trenčín, SK-911 50, Slovakia*
[5] *FunGlass, Alexander Dubček University of Trenčín, Študentská 2, Trenčín, SK-911 50, Slovakia*
[6]*Department of Biology, University of Hradec Králové, Rokitanského 62, 500 03 Hradec Králové, Czech Republic*
[7]*Department of Physics, University of Hradec Králové, Rokitanského 62, 500 03 Hradec Králové, Czech Republic*
[8]*Department of Medical Biophysics, Faculty of Medicine in Hradec Králové, Charles University,500 03 Hradec Králové, Czech Republic*

Abstract

The self-plasticization, i.e., the increase in the polymer segmental mobility by the inclusion of its own monomer, has a major impact on the structural, thermal, and mechanical properties of the polymer. Differential scanning calorimetry (DSC) was used to investigate the influence of thermally induced self-plasticization on the structural relaxation of polydioxanone (PDX). Depolymerization (based dominantly on the end-chain scission mechanism) was found to be controlled by the depolymerization temperature T_d as well as the actual number of re-melting cycles (while keeping the time spent at T_d constant). PDX samples with the glass transition temperature (T_g) ranging from −52 (highly plasticized) to −13 °C (virgin) were prepared. The DSC data were described in terms of the Tool-Narayanaswamy model; a consistent structural relaxation behavior associating the degree of

[*] Corresponding author: Tel.: +420 466 037 346 E-mail address: roman.svoboda@upce.cz

plasticization with T_g was identified. The activation energy first decreased with plasticization from 430 kJ·mol^{-1} to 210 kJ·mol^{-1} in the T_g range of −40 to −13 C, which is consistent with the plasticization-caused spacing-apart of the polymer chains resulting in larger free volume and increased freedom for the relaxation movements. For the highly plasticized PDX samples, the activation energy increased from 210 kJ·mol^{-1} to 310 kJ·mol^{-1}, which appears to be associated with the possible segregation of the portion of the plasticizer into a discrete phase. The width of the relaxation times distribution increased with plasticization as a consequence of the plasticizer loosening the polymeric chains and enabling a wider variety of the segmental movement. The plasticization also leads to a higher dependence of the segmental relaxation movements on their current physico-chemical and steric surrounding.

Keywords: self-plasticization; polydioxanone; DSC; structural relaxation; depolymerization

1. Introduction

Plastics are the most commonly used materials of the nowadays society. Their yearly production for 2021 was estimated to be over 390 million tons; the amount of produced plastics has been continuously growing for the last two decades. [1, 2] It is predicted that the overall accumulated amount of plastic waste will reach 3.4 billion tons by 2050. [3] In accordance with the concept of sustainable development, the circular economy model is being widely adopted by all major countries across the globe. The key aspect of this concept is the recycling of plastics. [4] Whereas plastics recycling was initially the domain of specialized large-scale industrial companies, the invention of 3D printing technologies [5 - 10] paired with the production of accessible table-top extruders has introduced the option of small-scale plastics recycling/reusing to numerous segments of industry, services, research and development, as well as to the common household usage. [11 - 20] This revolution in plastics

reusing, together with the current focus on the rapid development of biodegradable polymers, has led to the emergence of countless self-developed and untested procedures for plastics re-melting and high-temperature re-shaping. Inevitably, the most suitable polymeric materials are being pushed to the limits of their endurance and sustainability, which can lead to their slow high-temperature degradation/depolymerization during repeated processing [21 - 25]. Depending on the dominant depolymerization mechanism (chain-end scissions vs. random scission) [26, 27], a significant amount of monomers or low-mass oligomers can be released, which can induce the plasticization effect [28, 29].

The self-plasticization, i.e., the increase in the mobility of the polymer segments by incorporation of own monomer units in-between the polymer chains, can have major consequences with regard to the mechanical properties of the polymeric material [30 - 32]. One of the key phenomena defining the behavior of amorphous and semi-crystalline polymers is the glass transition [33 - 35] characterized by the glass transition temperature (T_g), i.e., the temperature at which an amorphous polymer changes from a hard/glassy state (below T_g) to a soft/leathery state (above T_g). The glass transition kinetics is driven by the structural relaxation processes, which are significantly affected by plasticization. The mechanisms interlinking the plasticization and structural relaxation processes were studied numerous times (see, e.g., [36 - 43]), providing the following conclusions: 1) plasticization decreases T_g; 2) plasticization decreases the relaxation time and promotes the relaxation of stresses; 3) plasticization (as opposed to anti-plasticization [37]) is associated with small flexible molecules with weak attractive forces towards the polymer chains, and as such decreases fragility [44] in the undercooled liquid state; 4) plasticization decreases the activation energy of segmental relaxation above T_g, whereas the activation energy does not change with plasticization below T_g; 5) plasticization was reported to both increase and decrease the size of cooperativity domains by decreasing the strength and frequency of intermolecular

interactions; 6) plasticization broadens the distribution of relaxation times (characterized by the KWW function [45, 46]) in amorphous matrices.

Despite the intense research, the detailed intricacies of the mutual inter-relationships between plasticization and structural relaxation are still not clearly understood. One of the main issues seems to be the focus only on selected aspects of the structural relaxation process. In the present paper, the effect of thermally induced self-plasticization on the structural relaxation process occurring in the glass transition range will be explored. Polydioxanone (PDX), a biodegradable poly(ester-ether) prepared by ring-opening polymerization of *p*-dioxanone (see Fig. 1) [47 - 49] and utilized in numerous medical applications [50 - 57], will be used as a model material. The main reason for the choice of PDX was its apparent strong inclination to the thermally induced end-chain scission, which produces large numbers of monomer units and is ideal for the self-plasticization research. In addition, at high temperatures, PDX does not burn but only depolymerizes and consequently evaporates – so no competition or masking of the plasticization effects by the generation of char or tar can occur.

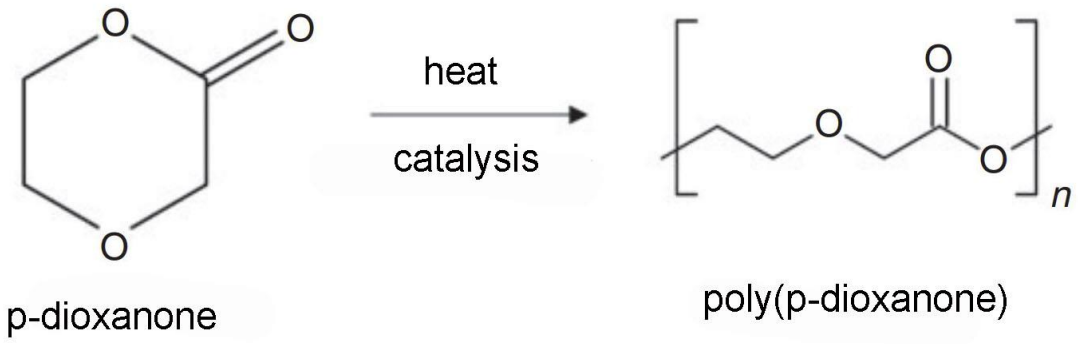

Fig. 1: Chemico-structural representation of PDX synthesis.

2. Experimental

The polydioxanone material was purchased in the form of a surgical suture from the SMI AG (St. Vith, Belgium) manufacturer. The material in the form of monofilaments with ~ 0.5 mm diameter was cut into approx. 3 mm long pieces that were further used for the calorimetric measurements. The differential scanning calorimetry (DSC) experiments were performed by a heat flow DSC Q2000 instrument (TA Instruments, USA) equipped with an autosampler, RCS90 cooling accessory, and T-zero technology; the instrument was calibrated using the In, Zn, and H_2O standards. For each set of measurements, 7 (3 mm) pieces of the PDX monofilament were weighted (with a ± 0.01 mg accuracy) and inserted in a hermetically sealed low-mass pan (ensuring a reproducible static air atmosphere). Selected datasets were reproduced using the differential scanning calorimeter DSC Pyris 1 (Perkin Elmer) equipped with the 2P intracooler – the power-compensation design of the instrument was utilized to rule out any major data distortions potentially produced by the heat-flow DSC Q2000.

Three series of temperature programs were realized in the DSC instrument to explore the depolymerization kinetics and to achieve various degrees of partial depolymerization associated with different levels of the monomer/plasticizer content:

1) In the first series, the temperature program was based on 50 cycles, where the sample was repeatedly re-melted at the depolymerization temperature T_d for the depolymerization time t_d = 5 min, cooled at 50 °C·min^{-1} below the glass transition temperature T_g, and heated back to T_d at 20 °C·min^{-1}. In this type of experiment, the applied depolymerization temperatures were T_d = 110, 130, 150, 170, and 190 °C.

2) The second series of the depolymerization temperature programs utilized a similar concept with T_d = 190 °C and t_d = 5 min. Here, the variable was the number of degradation cycles – the utilized values were 10, 20, 30, 40 (and 50 from the first series of temperature programs).

3) In the third series, several supplemental temperature programs were realized, providing deeper insight into the depolymerization kinetics: a) 25 degradation cycles, T_d = 190 °C and t_d = 5 min; b) 4 degradation cycles, T_d = 190 °C, and t_d = 62.5 min; c) 4 degradation cycles, T_d = 150 °C and t_d = 62.5 min.

Each of the above-mentioned temperature programs was performed for a fresh PDX sample. For each sample performed within the first and second series of temperature programs, two sets of structural relaxation DSC experiments were realized. The first set of structural relaxation experiments was based on the cyclic constant ratio (CR) measurements [58], where the sample was repeatedly cooled and heated through the glass transition region. The applied cooling and heating rates were 0.5, 1, 2, 3, 5, 7, and 10 °C·min^{-1}. The heating rate was always the same as the preceding cooling rate. The second set of the structural relaxation experiments was based on the constant heating rate (CHR) cyclic experiments [59], which are similar to the CR cycles, with the only difference being that the heating rate is for all cycles through the glass transition always similar (in the present study equal to 10 °C·min^{-1}). Before each set of the structural relaxation experiments (i.e., once before the CR cycles and a second time before the CHR cycles), the sample was freshly re-melted (1 min at 130 °C) to ensure a fully amorphous PDX matrix. Note that the virgin PDX crystallizes at laboratory temperature, and the crystallization onset further decreases with the degree of depolymerization [60]; the upper-temperature limits during the CR and CHR relaxation experiments thus had to be closely monitored and adjusted to avoid the crystal growth in the amorphous matrix.

Overall, 10 sets of CR and CHR cyclic experiments were realized for the PDX materials with different degrees of depolymerization (1 virgin/untreated PDX sample, 5 samples within the first series of temperature programs, 4 samples within the second series of temperature programs). The reproducibility of the DSC measurements was tested intrinsically within each set of measurements (either degradation cycles or the CR and CHR cycles) via

repeatability of the baselines and onsets of the relaxation peaks. In addition, for the degradation cycles, the reproducibility was directly confirmed during the second series of depolymerization temperature programs.

In addition to the DSC measurements, size exclusion chromatography (SEC) equipped with a multi-angle light scattering detector (MALS) was used to determine the molar mass distribution. In this regard, the following instrumentation was used: Agilent 1200 Series Isocratic Pump and Agilent 1200 Series Autosampler; a MALS detector HELEOS and a differential refractometer (RI detector) Optilab T-rEX, both from Wyatt Technology. Data acquisition and evaluation were performed using the ASTRA software from Wyatt Technology. Two Shodex HFIP-806 M 300 × 8 mm columns with hexafluoroisopropanol (HFIP) at a flow rate of 1 $ml \cdot min^{-1}$ as mobile phase were used for the separation. The samples were prepared as solutions in HFIP at a concentration of ≈ 4 $mg \cdot ml^{-1}$ and dispensed in volumes of 100 µl. The used HFIP was modified by the addition of 0.02 M CF_3COONa.

The structural arrangement of the selected PDX samples was investigated by means of Raman spectroscopy, using the DXR2 Raman microscope (Nicolet, Thermo Fisher Scientific) equipped with a 785 nm excitation diode laser (30 mW source, laser spot size 1.6 µm) and a CCD detector. The settings for the Raman measurements were: 20 mW laser power on the sample, 1 s duration of a single scan, and 100 scans accumulated in one spectrum.

3. Results

Differential scanning calorimetry was used to prepare PDX samples with different degrees of depolymerization. The DSC records of the degradation cycles performed within the first series of the degradation temperature programs are shown in Fig. 2. A typical cyclic degradation behavior is shown in Fig. 2B, where during the first cycle, the sample cooled at 50 $°C \cdot min^{-1}$ from 130 °C to −50 °C exhibits only the endothermic glass transition (with the

glass transition temperature $T_g \approx -20$ °C) with no traces of preceding crystal growth. During the consequent heating step, glass transition occurs at ~ −10 °C, followed by a strong exothermic crystallization peak (onset near 35 °C and peak at 53 °C) and a correspondingly pronounced endothermic melting peak with the extrapolated onset T_m = 96 °C. At temperatures just below T_m, the softening of the polymeric material leads to an additional reorganization of its structure, represented by the weak exothermic signal corresponding to an additional amorphous-to-crystalline transformation. Note that PDX is naturally a semi-crystalline polymer with a crystallinity degree of 45 – 55 % [61]. With the increasing degree of PDX depolymerization, which results in the increasing content of the plasticizing *p*-dioxanone monomer [62, 63], the T_g slightly decreases, the main crystallization peak (as well as the small exothermic peak preceding the melting) increases in magnitude and shifts to the lower temperature, and the melting peak correspondingly increases in magnitude and T_m decreases very slightly.

With the increasing depolymerization temperature T_d, the shift of all thermo-kinetic phenomena (glass transition, cold crystallization from the amorphous state, hot crystallization from the liquid state, melting) to the progressively lower temperatures occurs. For T_ds equal to 170 and 190 °C, the amount of the contained monomer is large enough for a small portion of the crystalline phase to be formed already during the rapid cooling. For the set of 50 depolymerization cycles performed with T_d = 190 °C and t_d = 5 min (overall time of depolymerization at T_d equal to 250 min), the released *p*-dioxanone already forms a separate phase able to crystallize and melt – as evidenced by the melting peak at ~ 15 °C. Another important finding resulting from the comparison of Figs. 2C and 2D is that the depolymerization proceeds more rapidly in conjunction with the repeated reorganization (crystallizations followed by re-meltings) of the polymeric matrix. Note that although the overall degradation time was 250 min in both cases, the shifts of the characteristic

temperatures and the corresponding phenomena to lower T were significantly greater in the case of many short cycles (as opposed to a few long depolymerization periods).

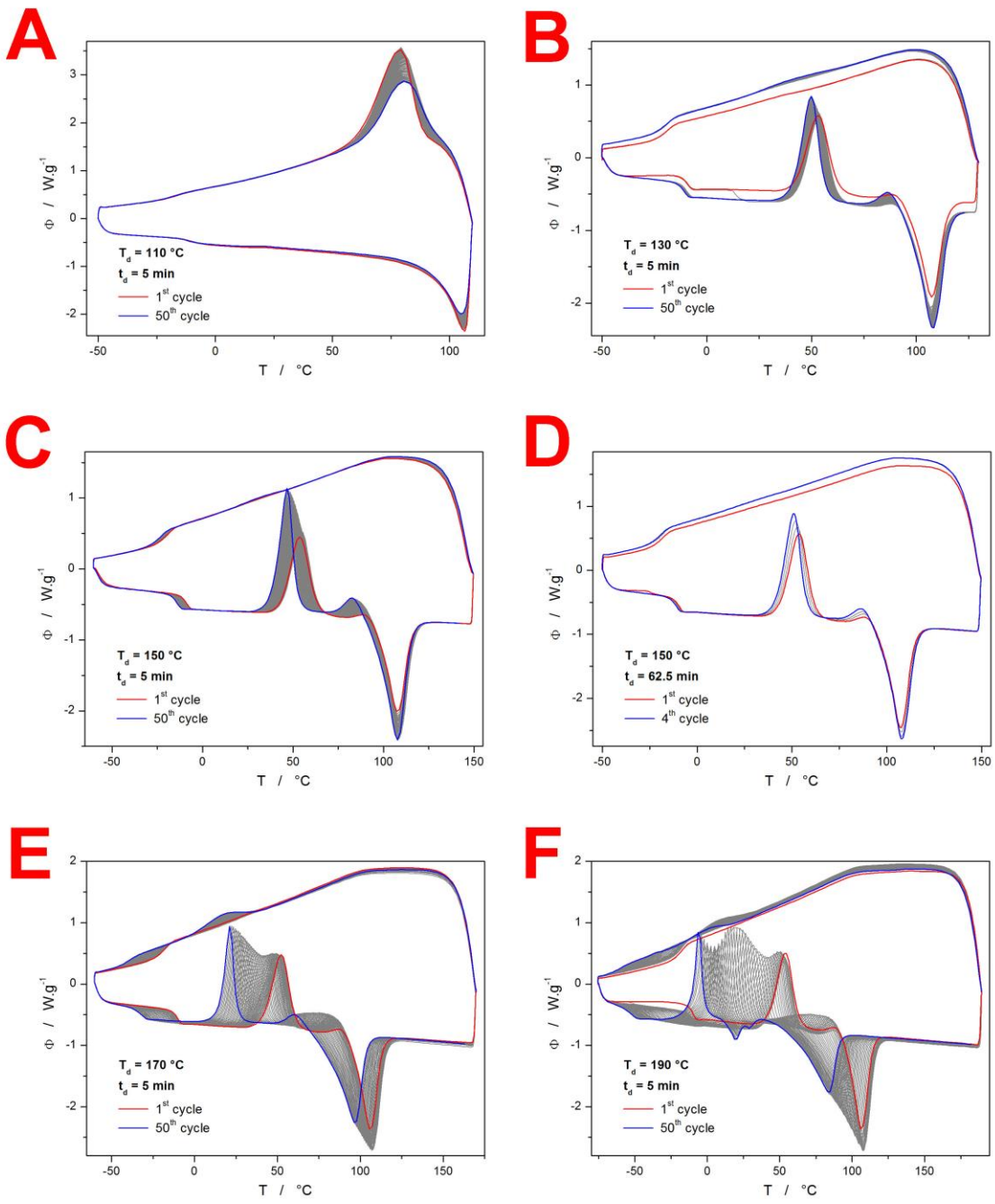

Fig. 2: A - F) Gradual depolymerization DSC experiments with repeated annealing (the duration of t_d) at the depolymerization temperature T_d in-between each cooling-heating cycle. The first and last cycles of each series are marked in color. The upper and lower parts of the DSC cycles correspond to the cooling and heating segments, respectively. Exothermic signals evolve in the upwards direction.

This is particularly important with respect to T_g, which is directly related to the plasticization intensity and, thus, the *p*-dioxanone concentration. As a consequence, for a

quantitative evaluation, it is suitable to perform only cyclic depolymerization programs with a uniform value of t_d. The last crucial information derived from Fig. 2, depicted in graph A, is that the melting of PDX is relatively slow. Despite the melting being already initiated at T_d = 110 °C and t_d = 5 min being perceivingly long enough for the sample to fully melt, a significant portion of the crystalline phase still apparently remained in solid form and instantly initiated the formation of the crystalline phase during cooling. As the PDX sample depicted in Fig. 2A exhibited "full" crystallization (no further exothermic signals are present during the consequent heating), the clear occurrence of the glass transition effect unambiguously confirms the semi-crystalline nature of PDX.

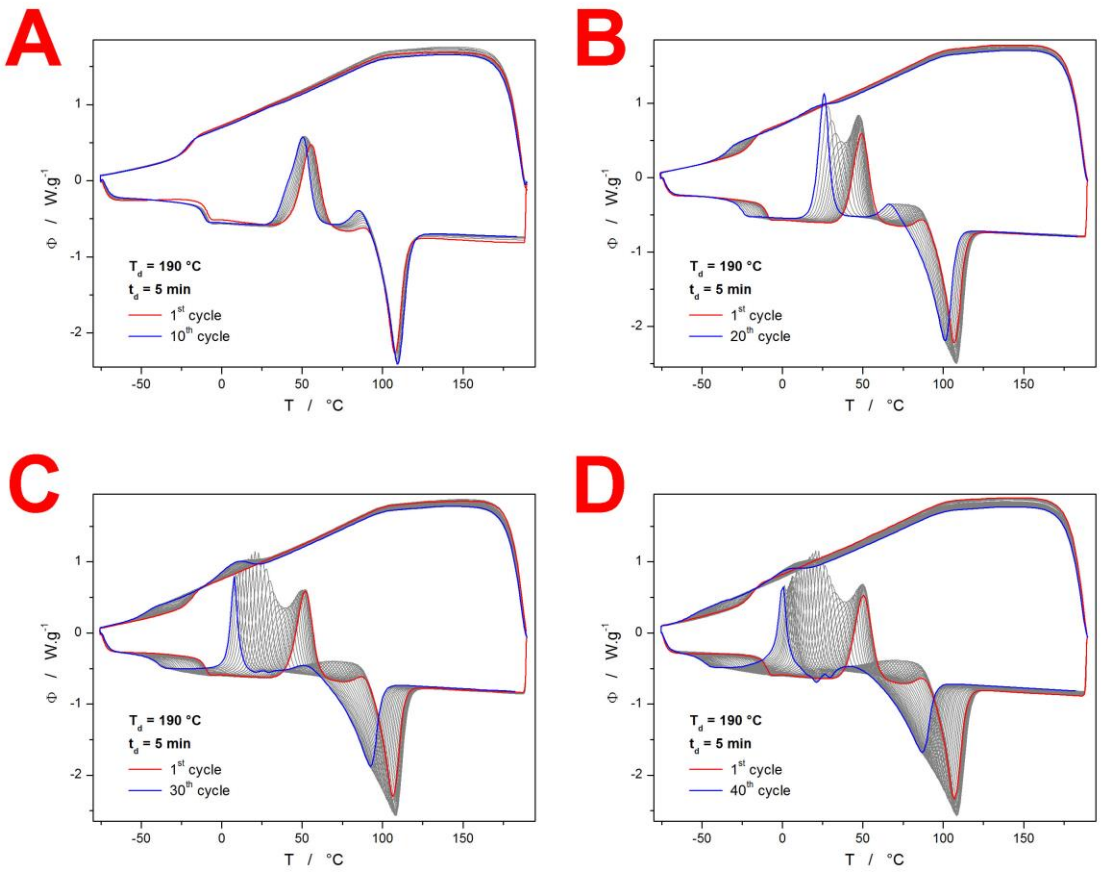

Fig. 3: A - D) Gradual depolymerization DSC experiments with repeated 5 min annealing at the depolymerization temperature 190 °C in-between each cooling-heating cycle. The graphs differ in the number of DSC cycles. The first and last cycles of each series are marked in color. The upper and lower parts of the DSC cycles correspond to the cooling and heating segments, respectively. Exothermic signals evolve in the upwards direction.

The DSC records of the degradation cycles performed within the second series of the degradation temperature programs are shown in Fig. 3. Similar evolution of the thermo-kinetic phenomena occurs with the increasing number of depolymerization cycles as did with increasing T_d. Whereas the rate of depolymerization is expected to be non-linear with T_d (one would assume an exponential Arrhenian dependence [64]), a non-linear relationship also occurs between T_g and the number of identical cycles (constant T_d and t_d). This nonlinearity is demonstrated by the following data extracted from Figs. 3 and 2F: 0 cycles ($T_g \approx -9$ °C), 10 cycles ($T_g \approx -11$ °C), 20 cycles ($T_g \approx -26$ °C), 30 cycles ($T_g \approx -40$ °C), 40 cycles ($T_g \approx -50$ °C), 50 cycles ($T_g \approx -55$ °C). A clear extreme (maximum rate of T_g decrease) occurs near 20 depolymerization cycles. This finding can probably be attributed to the evolving effect of the plasticizer amount on the displacement of the polymeric chains. Assuming that the rate of depolymerization is constant at the given T_d and no autocatalytic increase in the depolymerization rate occurs, the initial small decrease in T_g can be attributed to the small concentration of the monomer (*p*-dioxanone), which is not sufficient for a proper spacing-apart of the polymer chains, allowing better segmental movement. At further increase in the monomer content (after 20 depolymerization cycles), a large decrease in T_g occurs in correspondence with the sufficient amount of the plasticizer being embedded between the polymer chains for the proper loosening of the polymeric matrix. However, with the additional release of the *p*-dioxanone monomers, the rate of the T_g decrease slows down. This slow-down is probably associated with the polymeric matrix being gradually saturated with the plasticizer, where a certain (increasingly larger) portion of the *p*-dioxanone molecules does not contribute to the creation of the free volume/space between the polymer chains that gets translated into the segmental movement. At 50 depolymerization cycles and T_g of ~ -55 °C, the polymeric matrix starts to be apparently saturated (the T_g decrease rapidly ceases).

This explanation will be referred to and discussed several times throughout the paper. The evolution of T_g in for both data series depicted in Fig. 4

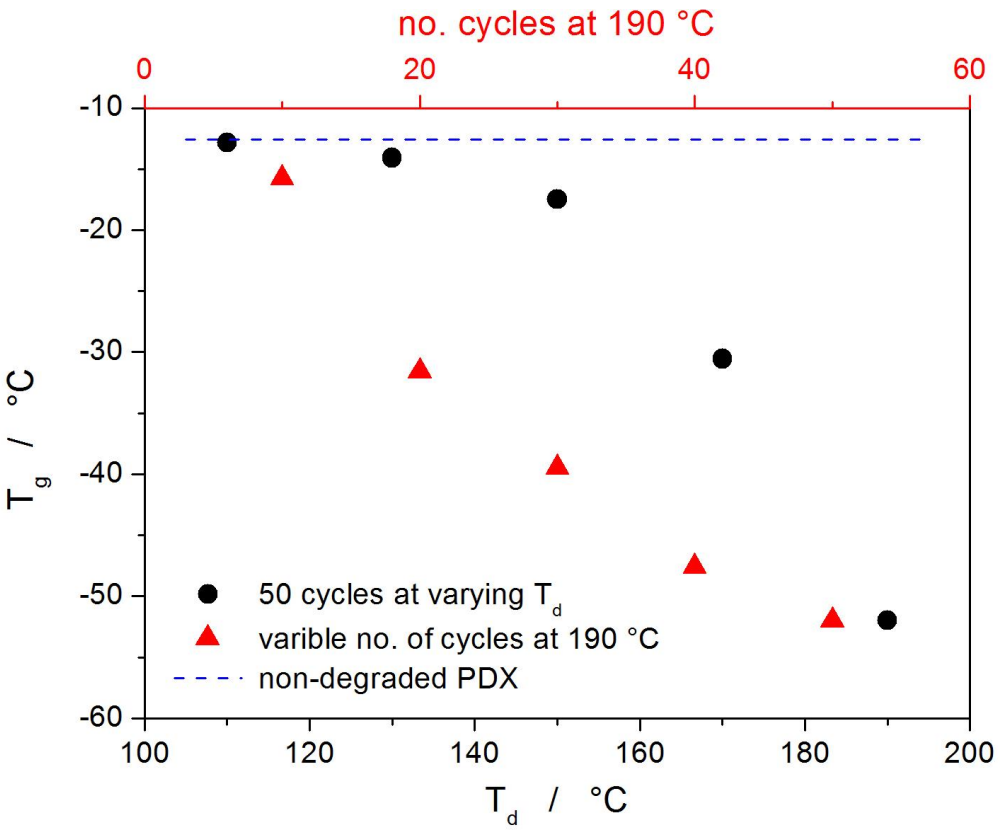

Fig. 4: Evolution of T_g within the two plasticization data series.

Examples of the full sets of the CR cycles measured for the weakly and strongly depolymerized PDX samples are shown in Fig. 5. The upper half of the curves corresponds to the cooling steps (the higher the curve, the higher the cooling rate); the lower half of the curves corresponds to the heating steps (the lower the curve, the higher the heating rate). Apart from the evident shift of T_g to the lower temperatures, the height/magnitude of the relaxation peak observed during the heating steps decreases with the plasticizer content (the width of the glass transition effect remains roughly similar, equal to ~ 15 – 20 °C). Note that during the CR cycles, the height of the normalized relaxation peak, in theory, changes only with the q^-/q^+ ratio and thus should remain similar for all cycles performed within each set.

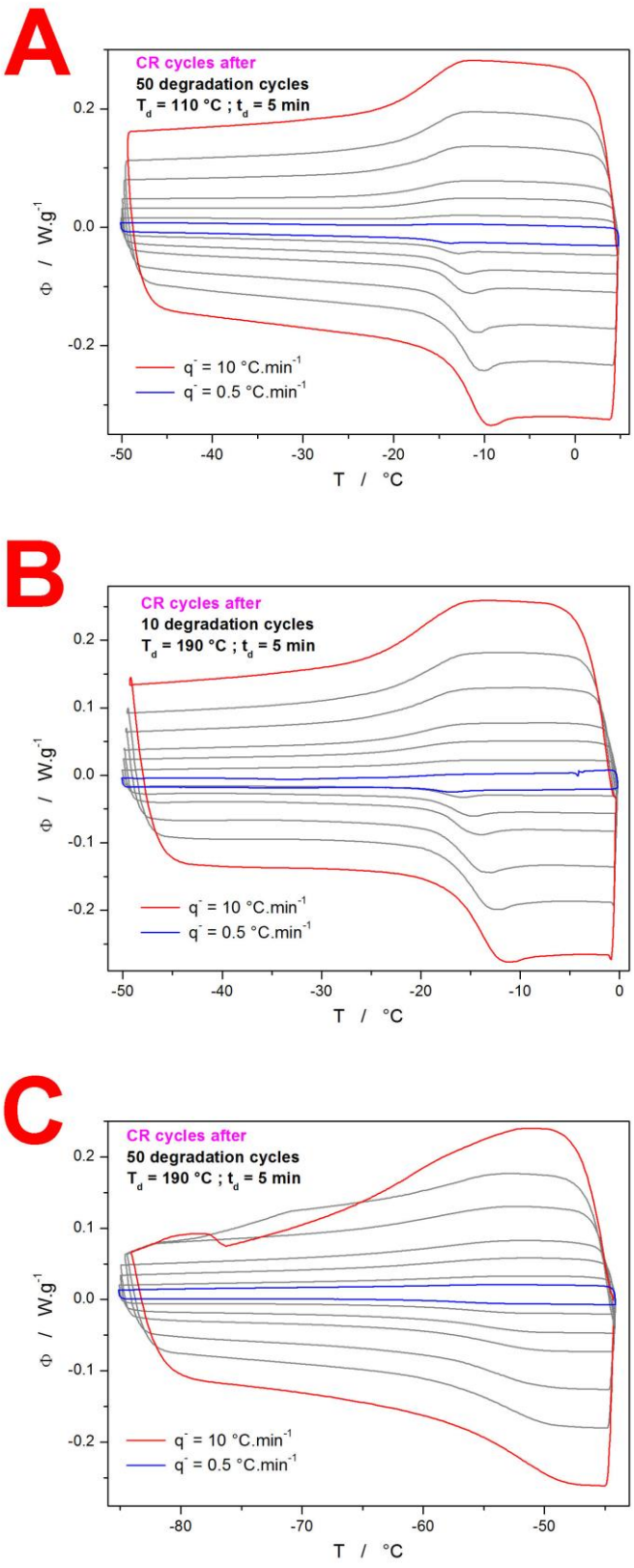

Fig. 5: A - C) Examples of the CR cycles being applied for selected partially depolymerized PDX samples. The first and last cycles of each series are marked in color and denoted by the applied cooling rate q^- (the magnitude of which is similar to that during the consequent heating step). The upper and lower parts of the DSC cycles correspond to the cooling and heating segments, respectively. Exothermic signals evolve in the upwards direction.

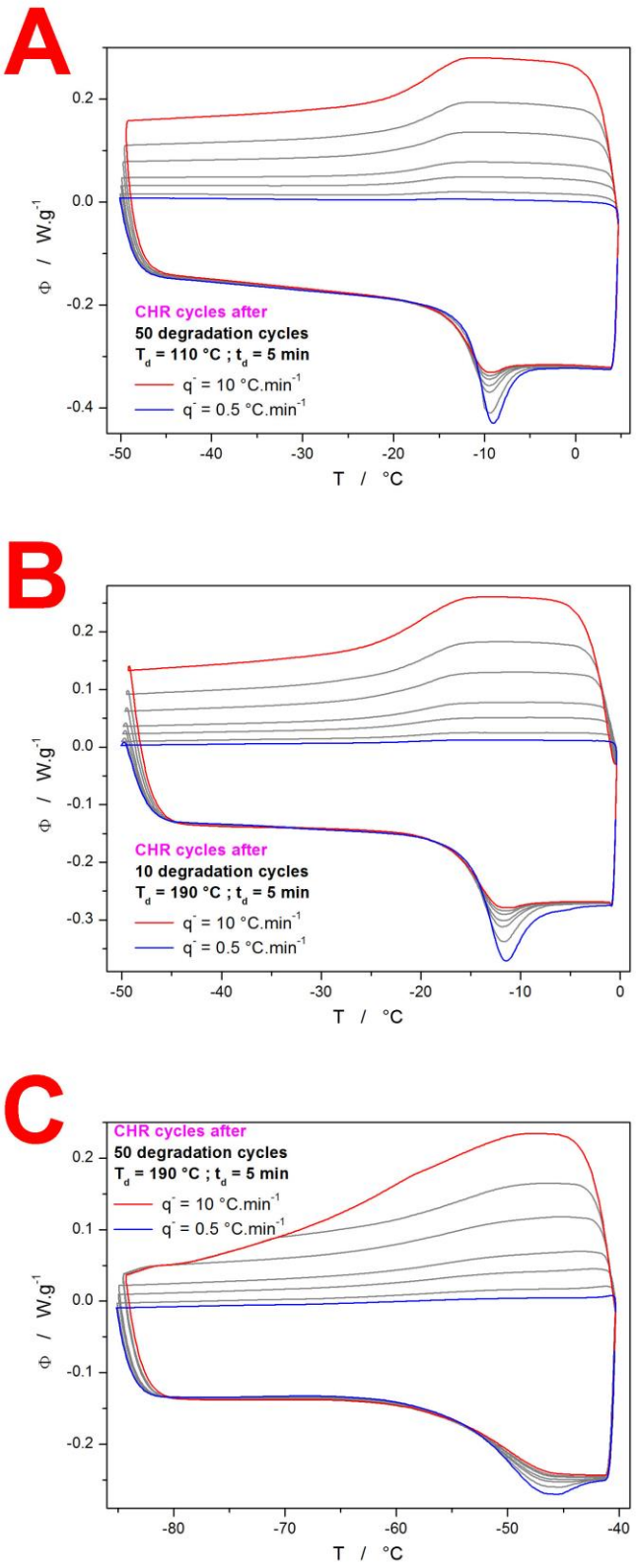

Fig. 6: A - C) Examples of the CHR cycles being applied for selected partially depolymerized PDX samples. The first and last cycles of each series are marked in color and denoted by the applied cooling rate q^- (heating steps were performed at q^+ = 10 °C·min^{-1}). The upper and lower parts of the DSC cycles correspond to the cooling and heating segments, respectively. Exothermic signals evolve in the upwards direction.

The decrease in the relaxation peak is even more evident in the case of the CHR cycles – see Fig. 6 for the sets of CHR cycles obtained for the samples with similar degrees of depolymerization as in Fig. 5. Indeed, for the sample with the highest plasticizer content (see Fig. 6C), the height of the relaxation peak (relative to the Δc_p difference between the glassy and undercooled liquid states) practically halves. These phenomena (shift of the glass transition in temperature and change in the relaxation peak height) determine the glass transition kinetics; their quantification and evolution with the plasticization degree will be discussed in Section 4.

The structural ordering of the PDX samples with different degrees of depolymerization was investigated by means of Raman spectroscopy. The full and zoomed-in Raman spectra obtained for selected depolymerized PDX samples are shown in Figs. 7A and 5B, respectively. The main depicted Raman signals can be identified followingly: the 870 cm^{-1} band corresponds to the C–O–C symmetric stretching vibration; the 1048 cm^{-1} band corresponds to the stretching vibration of C–C in the aliphatic chain; the 1451 cm^{-1} band corresponds to the $–CH_2–$ bending vibration; the 1732 cm^{-1} band corresponds to the C=O stretching vibrations in the ester carbonyl group; the 483, 1242, 1403, 1610, and 1638 cm^{-1} bands correspond to the vibrations in the Solvent Violet 13 (dye) structure [65 - 68]. It was found [60, 65, 66] that the shoulder of the 1732 cm^{-1} band corresponds to the C=O vibrations in the amorphous phase, whereas the sharp/main band represents the signal from the crystalline phase. The Raman spectra of the PDX samples with different degrees of depolymerization exhibit high similarity with regard to the presence/absence of particular bands, which indicates that no significant decomposition or oxidation reactions take place in PDX at the tested high temperatures. The zoomed-in graph (Fig. 7B) depicting the 1732 cm^{-1} band testifies about the degree of crystallinity characteristic for the various levels of PDX depolymerization. Note that PDX is a naturally semi-crystalline polymer [50], which

crystallizes even from a fully amorphous state at laboratory temperature. The decreasing magnitude of the shoulder (corresponding to the amount of the contained amorphous phase) at the 1732 cm^{-1} band indicates that with increasing T_d, the equilibrium amount of the amorphous phase decreases. This is in good correspondence with the depolymerization-caused higher tendency towards crystallization (see Figs. 2 and 3), as well as with the assumed preference of the depolymerization in the amorphous phase due to its generally higher reactivity.

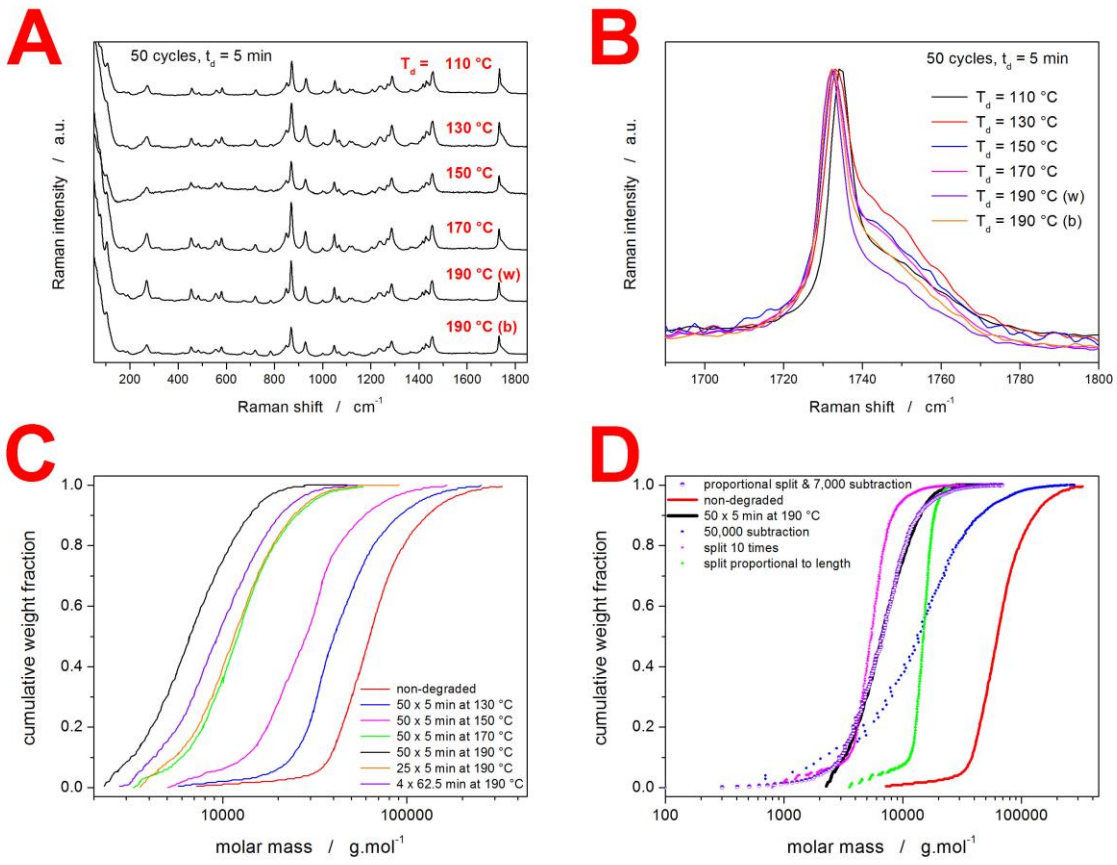

Fig. 7: A) Raman spectra of the selected partially depolymerized PDX samples. The spectra differ in applied T_d; the labels "w" and "b" correspond to the white and black domains of the sample, respectively.
B) Raman spectra from graph A zoomed-in on the 1732 cm^{-1} band.
C) The cumulative weight distribution of molar masses for the selected partially depolymerized PDX samples.
D) Theoretically simulated cumulative weight distributions of molar masses (points) originating from the virgin/non-degraded PDX (red curve) and compared to the sample depolymerized during 50 5 min cycles at 190 °C (black curve). See the text for the details of the simulations.

The only exception in the above-suggested trend is the indicated low amount of the amorphous phase for the sample depolymerized at T_d = 110 °C (the content of the amorphous phase appears to be similar to that of the sample cycled to T_d = 190 °C). This is probably a consequence of the sample being repeatedly not fully melted at 110 °C, which led to the consequent rapid crystallization already during the cooling (a higher degree of achieved crystallinity during the slow cooling of a melt is also reported in [60]). Contrary to the PDX samples depolymerized at lower temperatures, the depolymerization at 190 °C led to the formation of two color-distinguished phases (white "w" and black "b"). According to the Raman spectra, the white phase has a significantly higher content of the crystalline phase; the existence of the two phases may be associated with the possible segregation of the portion of the plasticizer into a discrete phase, as will be discussed later in Section 4.

The molar mass (M / g·mol^{-1}) changes with the gradual depolymerization were monitored by means of SEC-MALS – see Fig. 7C, where the cumulative weight fraction is plotted in dependence on the molar mass. The series of 50 cycles with 5 min at T_d per cycle show that the depolymerization significantly accelerates with T_d, with the highest apparent acceleration being observed between the T_ds 150 and 170 °C. Interestingly, a similar degree of depolymerization (and molar mass decrease) was recorded for the 50 cycles at T_d = 170 °C and for 25 cycles at T_d = 190 °C, indicating "only" doubling of the depolymerization rate between 170 and 190 °C. A very important finding is associated with the SEC-MALS measurement for the sample depolymerized during 4 cycles with 62.5 min at T_d = 190 °C. When compared with the standard series of 50 cycles with 5 min at 190 °C (in both cases, the depolymerization time is t_d = 250 min), it is clear that the repeated solidification and melting strongly enhance the depolymerization effect. The series of 4 cycles with 62.5 min at 190 °C led to a state that is slightly closer to that produced during 50 5 min cycles at T_d = 170 °C than that at T_d = 190 °C; we estimate that by this decrease in the number of re-meltings, the

effective T_d for the standard 50 5 min cycles was decreased by more than 10 °C, below T_d = 180 °C. Worth noting is also the cut-off of the low-M tail of the cumulative weight dependences. Note that the molar mass of 1 PDX mer is 102.088 $g \cdot mol^{-1}$.

In order to provide further insight into the depolymerization mechanism and confirm its dominant nature being the unzipping (chain-end scissions) process [62, 63], several basic simulations of the fundamental depolymerization mechanisms were performed – see Fig. 7D. The input data curve was that for the non-degraded (virgin) PDX sample; the results of the simulations were compared to the cumulative weight distribution dependence for the ultimate series of 50 5 min cycles at T_d = 190 °C. Simulations based on the sole unzipping mechanism (blue points in Fig. 7D) reveal that this depolymerization mechanism leads to a stretched sigmoidal dependence with a lower slope at the inflection point; the high-M end of the sigmoidal dependence changes its position only negligibly in the logarithmic scaling of the X-axis. Note that during the unzipping, all chain ends have a similar chance of being cut off; thus, a simple decrease/subtraction of a selected number of mer units (simplified to a given part of the molar mass in our case) from each molar mass fraction can truthfully represent this mechanism.

Opposed to the chain-end scissions, the random scission mechanism represents the splitting of the polymer chain at a random position inside the chain. The simplest forms of this mechanism, where the chain is split into similarly long pieces (i.e., the scission always occurs in the half-chain position), are in Fig. 7D represented by the pink and green data points. The pink stars correspond to a theoretical case, where the splitting would happen with the same probability for each chain (i.e., each chain splits into a similar amount of fragments regardless of its original length). The green triangles correspond to the situation, where the splitting happens with the same probability for each mer (i.e., proportional to the chain length, but still splitting the chains into equally long parts – a simplified version of the simulation).

Both these types of simulations lead to either no change or to an increase in the steepness and inflection slope of the sigmoidal dependence. By implementing both types of chain scissions into the simulation, the experimental dependence corresponding to the 50 5 min cycles at T_d = 190 °C was acceptably reproduced (considering the low-M detection limit of SEC-MALS method) – see the overlap of the black line and violet half-filled points. In this simulation, each chain was split only ~ 4 times, but the amount of the chain-end scissions required to reproduce the slope of the dependence was ~ 70 (subtraction of 7000 g·mol^{-1}). This proportion indicates that the chain-end scissions indeed represent the dominating type of the chain-shortening mechanism.

4. Discussion

The glass transition kinetics and evolution of the rate of structural movements are nowadays described by the phenomenological relaxation Tool-Narayanaswamy-Moynihan (TNM) model that can be expressed by the following equations [69 - 71]:

$$\Phi(t) = \exp\left[-\left(\int_0^t \frac{dt}{\tau(T,T_f)}\right)^{\beta}\right] \tag{1}$$

$$\tau(T,T_f) = A_{TNM} \cdot \exp\left[x\frac{\Delta h^*}{RT} + (1-x)\frac{\Delta h^*}{RT_f}\right] \tag{2}$$

where $\Phi(t)$ is the base relaxation function defined for the DSC measurements as $(c_p - c_{pg})/(c_{pl} - c_{pg})$. The c_{pg} and c_{pl} are the extrapolated heat capacities in the glass and undercooled liquid regions, respectively. The other involved quantities are time t, relaxation time τ, the parameter of non-exponentiality β ($0 < \beta \leq 1$), the pre-exponential factor A_{TNM}, the parameter of non-linearity x ($0 < x \leq 1$), the apparent activation energy of the structural relaxation Δh^*, the universal gas constant R, temperature T, and the fictive temperature T_f.

The recommended [72] approach to the enumeration of the TNM equations is based on the following sequence: 1) determination of Δh^* from the CR cycles; 2) determination of A_{TNM} based on non-linear optimization + identification of the potential artificial/instrumental distortions of the DSC data; 3) determination of β and x using the improved simulation-comparative method. Starting with the first step, the apparent activation energy Δh^* can be determined from the q^--based shift of the temperature corresponding to the maximum of the relaxation peak T_p during the CR cycles [73]:

$$-\frac{\Delta h^*}{R} = \left[\frac{d \ln|q^-|}{d(1/T_P)}\right]_{q^-/q^+=const} \tag{3}$$

where q^- corresponds to the cooling rate preceding the heating scan from which the T_p is determined; for practical purposes, q^+ is used/mentioned in the cases when $q^-/q^+ = 1$. The dependences represented by Eq. 3 are shown in Figs. 8A and 8B for the two series of depolymerized PDX samples (50 cycles at variable T_d vs. variable number of cycles at T_d = 190 °C). As the dependencies are fairly linear, no restrictive selection of the evaluated q^+ range was adopted. The spacing between the individual dependences well demonstrates the evolution of T_p (practically similar to T_g) with the degree of depolymerization. Contrary to the non-monotonous trend in the evolution of the cumulative molar mass, where a significant gap occurred between T_ds 150 and 170 °C (see Fig. 7C and the corresponding discussion), the decrease in T_g monotonously accelerates with T_d. On the contrary, it is the isothermal degradation kinetics (expressed by the change of T_g/T_p in Fig. 8B) that shows an extreme during the initial 20 cycles. The corresponding Δh^* values, determined by using Eq. 3 on the data from Figs. 8A and 8B, are depicted in Figs. 8C and 5D, respectively. The plasticization effect can evidently decrease the Δh^* of PDX by almost 50 %.

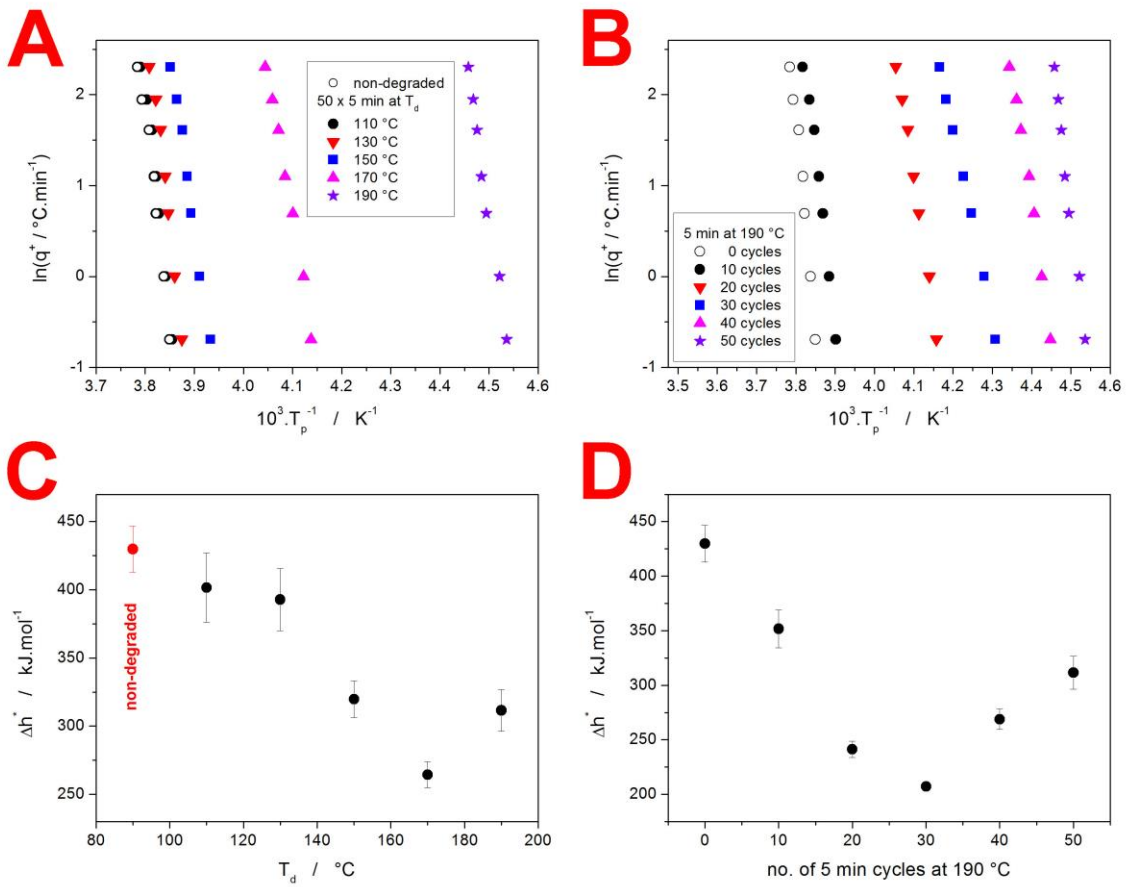

Fig. 8: A) Evaluation of the CR cycles (in accordance with Eq. 3) measured for the samples subjected to the 1st series of the depolymerization temperature programs.
B) Evaluation of the CR cycles (in accordance with Eq. 3) measured for the samples subjected to the 2nd series of the depolymerization temperature programs.
C) Δh^* values determined from graph A according to Eq. 3.
D) Δh^* values determined from graph B according to Eq. 3.

In the second step of enumerating Eqs. 1 and 2, the pre-exponential factors were determined by means of non-linear optimization based on the algorithms introduced in [74]. Note that the instrumental distortive effects of the Q2000 DSC do not affect the position of the glass transition effect on the temperature axis, and thus an accurate determination of A_{TNM} is possible. The pre-exponential factor values determined for the present PDX samples with different depolymerization degrees are summarized in Table 1.

Table 1

Values of the pre-exponential factor lnA determined by the non-linear optimization for the PDX samples with different degrees of depolymerization.

Temperature program	ln(*A*/s)
virgin PDX	−195.7
50 cycles, t_d = 5 min, T_d = 110 °C	−183.0
50 cycles, t_d = 5 min, T_d = 130 °C	−179.9
50 cycles, t_d = 5 min, T_d = 150 °C	−148.0
50 cycles, t_d = 5 min, T_d = 170 °C	−128.5
50 cycles, t_d = 5 min, T_d = 190 °C	−165.9
10 cycles, t_d = 5 min, T_d = 190 °C	−164.3
20 cycles, t_d = 5 min, T_d = 190 °C	−117.5
30 cycles, t_d = 5 min, T_d = 190 °C	−104.0
40 cycles, t_d = 5 min, T_d = 190 °C	−138.8

The Δh^* & A_{TNM} combinations were consequently used to simulate a dense matrix of theoretical CHR cycles data series, where the temperature program copied the one used for the actual experiments (see Section 2) and the input parameters were (in addition to the already determined Δh^* & A_{TNM}) different combinations of the parameters β and x (both varied from 0.2 to 0.8 with a step of 0.05). In this way, 169 different sets of CHR cycles were simulated for each PDX sample defined by the characteristic Δh^* & A_{TNM} combination. These data were used as a basis for the simulation-comparative method [72, 75], which is built upon the comparison of the experimentally determined and theoretically simulated values of the relaxation peak height C_p^{max}. This quantity is determined as follows:

$$C_p^{\max} = \frac{C_p^{T\max} - C_{pg}}{C_{pl} - C_{pg}} \tag{4}$$

where C_{pl} and C_{pg} are the extrapolated heat capacities in the liquid and glassy states, respectively, and C_p^{Tmax} is the heat capacity corresponding to the maximum of the relaxation peak (Eq. 4 effectively normalizes the Δc_p between 0 and 1). The evolution of the experimental C_p^{max} values is for both PDX depolymerization series shown in Fig. 9.

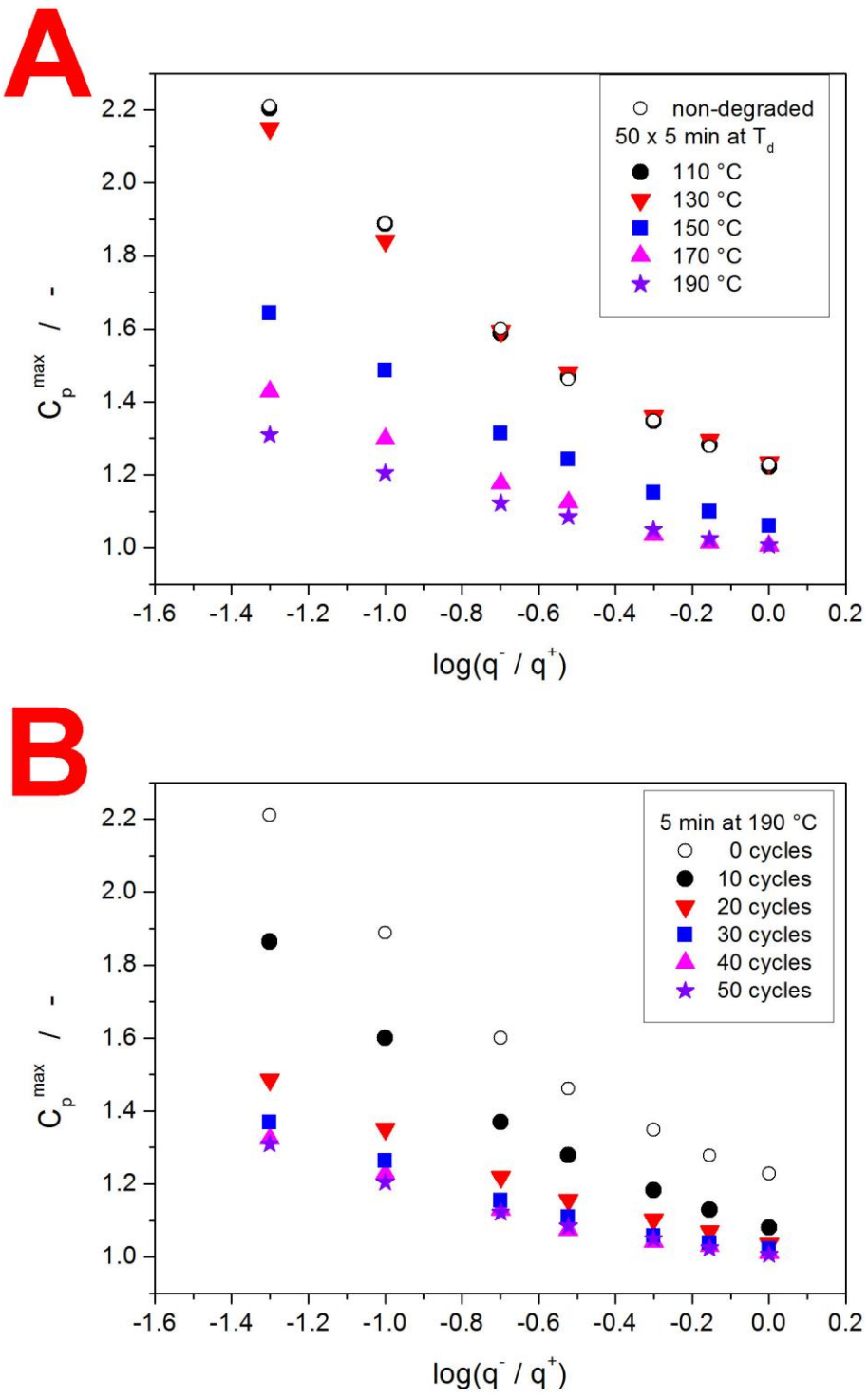

Fig. 9: A) C_p^{max} values determined according to Eq. 4 from the CHR cycles measured for the samples subjected to the 1st series of the depolymerization temperature programs.
B) C_p^{max} values determined according to Eq. 4 from the CHR cycles measured for the samples subjected to the 2nd series of the depolymerization temperature programs.

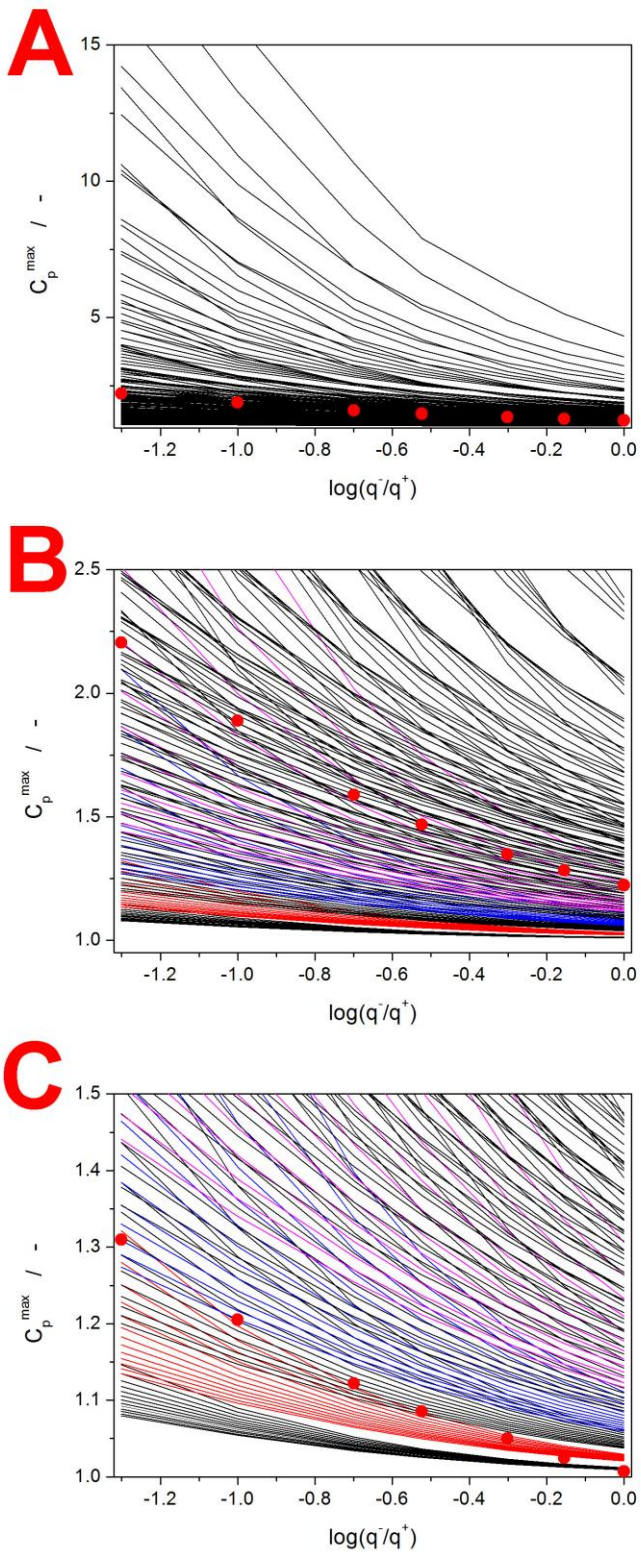

Fig. 10: Schematic visual representation of the application of the simulation-comparative method to the selected sets of CHR cycles measured for partially depolymerized PDX samples. Points represent experimental data; lines correspond to the C_p^{max}–log(q^-/q^+) dependences theoretically simulated for different β&x combinations (Δh^* and ln$A$ input into the simulations were determined for each set of experimental CHR cycles prior to the application of the simulation-comparative method). Colors in graphs B and C correspond to the different β sets (the lower the C_p^{max}, the lower the β). Within each β set, the non-linearity parameter x decreases as C_p^{max} increases.

Apparently, the height and the overall shape of the relaxation peak do not change even during relatively long depolymerization at 130 °C, which may indicate a threshold for the macroscopic manifestation of the depolymerization kinetics. These dependencies are then compared to the theoretical data simulated [74, 75] for the identical temperature program, corresponding Δh^* & A_{TNM} values (these quantities need to be determined beforehand), and various combinations of β and x. The best fit can be evaluated either visually or numerically (as was the present case, using the minimum value of the sum of squared residue). In Fig. 10, example comparisons of experimental and theoretically simulated data are shown to demonstrate the density of the simulated data-curves matrix. The method can be further improved by considering additional characteristic parameters of the relaxation curves (apart from C_p^{max}) or by combining the algorithm with iterative visual (performed manually) verification of the overall shape of the CHR cycles set.

The ultimate outcome of the above-described methods, i.e., the TNM parameters obtained for the structural relaxation process in the PDX samples with different degrees of depolymerization (and plasticizer content), is shown in Fig. 11. Since two different series of depolymerization temperature programs were applied, the T_g value was chosen as a common denominator as it should best correspond to the amount of released/present mer *p*-dioxanone units. Starting with the apparent activation energy of structural relaxation Δh^* (see Fig. 11A), the increasing plasticizer content leads to a large decrease in Δh^* – from ~ 430 kJ·mol^{-1} for the virgin non-degraded PDX to ~ 210 kJ·mol^{-1} for the PDX with $T_g \approx -40$ °C. This agrees with the expectations; the plasticization-caused spacing-apart of the polymer chains results in larger free volume and increased freedom for the segmental relaxation movements. Interestingly, at higher plasticizer contents ($T_g < -40$ °C), the activation energy starts to increase again (at a higher rate than that of the preceding Δh^* decrease).

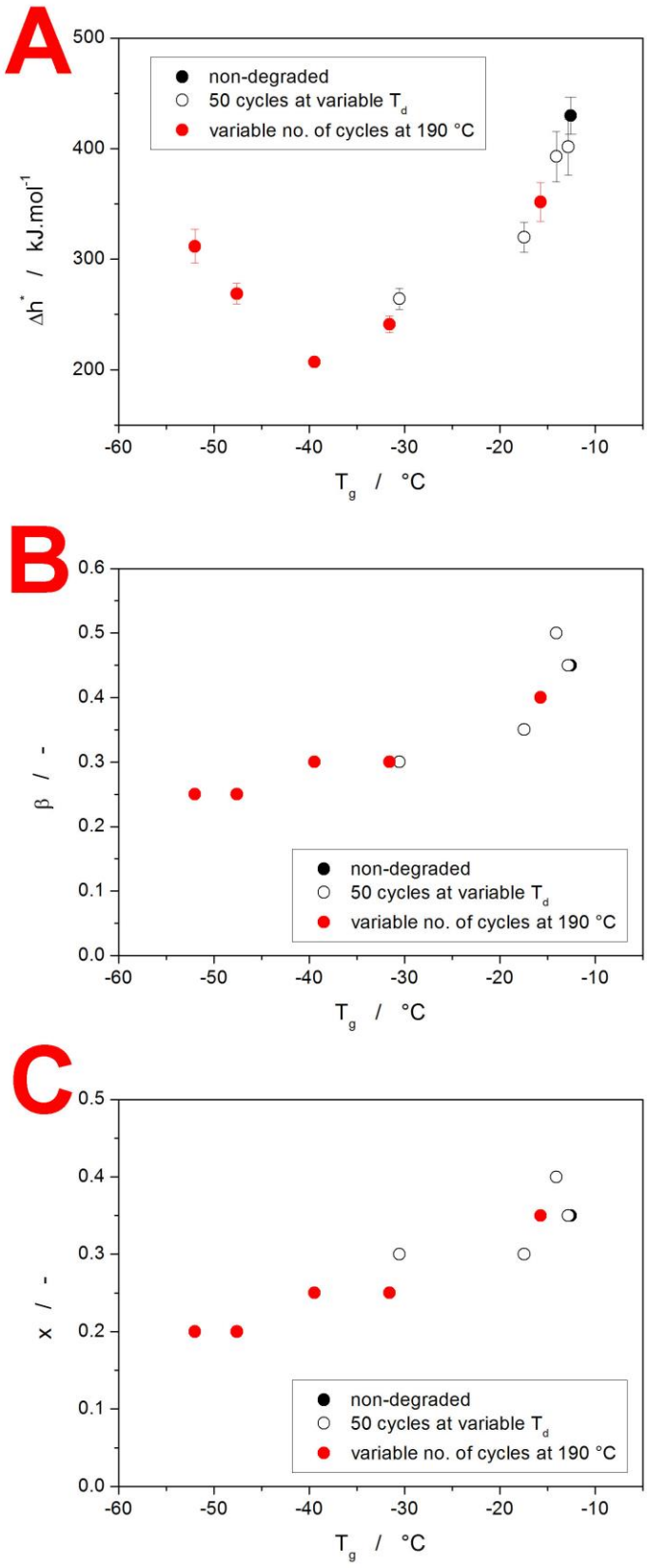

Fig. 11: Dependence of the TNM parameters (Δh^* in graph A, β in graph B, x in graph C) on T_g of the partially depolymerized PDX samples. Note that the data-point for 50 depolymerization cycles at T_d = 190 °C is shared by both datasets.

While revealing the essence of this Δh^* increase, the first idea was based on the potential change of the degree of crystalline content inevitably formed during the preparation of the (intended) amorphous phase after the intense depolymerization. As shown in Figs. 2 and 3, a small portion of the PDX material indeed crystallizes during the rapid cooling. However, the occurrence and intensity of the crystallization process are inconsistent with the discussed Δh^* increase – significant crystallization occurs already for the 50 5 min cycles at T_d = 170 °C, where the Δh^* still decreases ($T_g \approx -30.5$ °C). In addition, the amount of the crystalline phase formed during the preparation of the present highly depolymerized PDX samples is rather small. The achieved degrees of crystallinity χ_c were 6.7, 4.6, 3.4, and 1.3 % for the 50 cycles at T_d = 170 °C, 30 cycles at T_d = 190 °C, 40 cycles at T_d = 190 °C, and 50 cycles at T_d = 190 °C, respectively. As was shown in [60], Δh^* does not change with the increasing PDX crystallinity χ_c. On the other hand, the discussed Δh^* increase very well corresponds to the occurrence of the melting peaks of the *p*-dioxanone (PDX mer) – see Figs. 2 and 3 for the data on (30), 40, and 50 cycles of 5 min isotherms at 190 °C. The occurrence of the melting of the plasticizer indicates that the *p*-dioxanone crystallizes in a significant amount (not necessarily during the cooling/preparation of the amorphous phase), which is conditioned by its at least partial separation into a discrete phase. This possible segregation of the portion of the plasticizer may densify the domains with the remaining polymeric chains, which could lead to the increase in the activation energy for their movement. The continuous decrease in T_g could be, in such case, explained by either the Δh^* being dominantly driven by different complexity of relaxation movements compared to T_g or (more probably) by the high decrease in the molar mass partially mimicking the plasticizing effect (and thus contributing to the continued T_g decrease).

Contrary to Δh^*, the TNM parameters β and x show a monotonous decrease with the amount of present *p*-dioxanone plasticizer – see Figs. 11B and 11C. Also, in the case of these

parameters, the small amount of the crystalline phase does not significantly affect the structural relaxation kinetics. The non-exponentiality parameter β was in [60] (a study of structural relaxation in partially crystalline PDX samples) not affected by χ_c increasing up to 25 % of crystalline content, and the non-linearity parameter x only slowly gradually increased (by ~ 0.15 throughout the 0 – 25 % χ_c range). Hence, the trends depicted in Fig. 11 can again be attributed mostly to the effect of the present plasticizer. Bearing in mind that the non-exponentiality parameter β reflects the (inverted) distribution of the relaxation times in the amorphous matrix [33], its decrease from 0.45 to ~ 0.25 can be interpreted as an increased variability of relaxation movements being introduced into the system with the released plasticizer. This is well consistent with the idea of the *p*-dioxanone embedded between the polymeric chains, reducing intermolecular interactions and enabling a greater variety of segmental movement. The initial faster decrease in β then corresponds to the first formation of the loosened pockets/domains that are further extended with additionally increasing plasticizer content.

Regarding the non-linearity parameter x, it is generally interpreted as the measure of interconnectivity and of participation of larger structural entities in the structural relaxation processes ($\uparrow x \approx$ low participation of structural state and high participation of thermal vibrations). [33] In this context, the decrease in x with increasing *p*-dioxanone content can be perceived as an increasing influence of the current structural (dis)order on the relaxation movements. This may be counter-intuitive considering the large decrease in molar mass and general shortening of the polymeric chains, but the plasticization-initiated increase in the overall mobility of the polymeric segments may also lead to the possibility of their more intense interaction during the structural relaxation re-ordering.

5. Conclusions

The effect of self-plasticization on the structural relaxation process (proceeding in the glass transition range) was investigated for the polydioxanone polymer. The thermally induced self-plasticization was realized directly in the DSC cell by applying a variety of cyclic temperature programs. In this way, PDX samples with T_g ranging from −52 to −13 °C were prepared. The depolymerization rate appears to be controlled not only by the temperature but also by the number of re-melting cycles. One possible insight into this phenomenon (reserved for future investigation) may be represented by a higher chance for the random chain scissions (as opposed to the end-chain scissions) being associated with the re-melting/re-solidifying processes. The end-chain scission depolymerization mechanism was confirmed to be the dominant one for PDX, as the presence of large amounts of the *p*-dioxanone monomer was detected (via its DSC melting peak) for highly depolymerized samples.

Apart from the obvious large decrease in T_g, the effect of the self-plasticization on the structural relaxation process was expressed in terms of the evolving trends in the TNM model kinetic parameters. The activation energy was found to first decrease with plasticization (from ~ 430 kJ·mol^{-1} to ~ 210 kJ·mol^{-1}) in the −13 to −40 °C T_g range, which is consistent with the plasticization-caused spacing-apart of the polymer chains resulting in larger free volume and increased freedom for the relaxation movements. For the highly plasticized PDX samples (T_g in the −52 to −40 °C range), the Δh^* increases from ~ 210 kJ·mol^{-1} to ~ 310 kJ·mol^{-1}, which appears to be associated with possible segregation of the portion of the plasticizer into a discrete phase (evidenced by its suddenly highly increased tendency toward crystallization). The non-exponentiality parameter β decreases with plasticization from 0.45 to 0.25, which is consistent with the idea of the plasticizer loosening the polymeric chains and enabling a greater variety of the segmental movement. The non-linearity parameter x decreases with

plasticization from 0.35 to 0.2, which indicates a higher dependence of the segmental relaxation movements on their current physico-chemical and steric surrounding.

Can these findings be generalized to other polymeric materials? If we base the answer on the comparison of the present results with the main literature-reported links between the plasticization and structural relaxation (as presented in the introductory part), it can be concluded that the following statements are unambiguously confirmed by the current study: plasticization decreases T_g and the relaxation time in general; plasticization broadens the distribution of relaxation times. On the other hand, the present results, showing the non-monotonous development of the relaxation activation energy with the degree of plasticization, added even more complexity to the current state of knowledge, where the relevant studies have for other polymers so far reported either only monotonously increasing or decreasing Δh^*. Lastly, the present data also indicate that the plasticization increases the cooperativity during the relaxation motions of particular segments within the polymeric matrix – despite the fact that the molar mass largely decreases during the self-plasticization. This interpretation of the x-T_g plasticization is, however, relatively new [76], and requires further verification.

Acknowledgments

This work has been supported by the Ministry of Education, Youth and Sports of the Czech Republic (project LM2023037 and Cooperatio Program, research area DIAG). M.CH. thanks to The Slovak Grant Agency for Science for the support under Grant No. VEGA 2/0091/20, and APVV-21-0016.

Data availability

The data are available on request.

References

[1] Available online: https://www.statista.com/statistics/282732/global-production-of-plastics-since-1950/ (accessed on 27 July 2023).

[2] N.A. Samak, Y. Jia, M.M. Sharshar, T. Mu, M. Yang, S. Peh, J. Xing. Recent advances in biocatalysts engineering for polyethylene terephthalate plastic waste green recycling. Environ. Int. 145 (2020) 106144
[3] Available online: https://wrap.org.uk/blog/2021/02/shared-vision-more-sustainable-food-system-why-now-more-ever-weneed-courtauld (accessed on 27 July 2023).
[4] C. Zhu, T. Li, M.M. Mohideen, P. Hu, R. Gupta, S. Ramakrishna, Y. Liu. Realization of Circular Economy of 3D Printed Plastics: A Review. Polymers 13 (2021) 744
[5] H. Quan, T. Zhang, H. Xu, S. Luo, J. Nie, X. Zhu. Photo-curing 3D printing technique and its challenges. Bioact. Mater. 5 (2020) 110–115.
[6] Y. Zou, Q. Han, X. Weng, Y. Zou, Y. Yang, K. Zhang, K. Yang, X. Xu, C. Wang, Y. Qin, et al. The precision and reliability evaluation of 3-dimensional printed damaged bone and prosthesis models by stereo lithography appearance. Medicine 97 (2018) 9797.
[7] S. Jeong, J. Sim, H. Kim, D. Shin, D. Hong. Application of LOM for Freeform Architecture. J. Korean Soc. Precis. Eng. 34 (2017) 903–909.
[8] J. Jing, Y. Chen, S. Shi, L. Yang, P. Lambin. Facile and Scalable Fabrication of Highly Thermal Conductive Polyethylene/Graphene Nanocomposites by Combining Solid-State Shear Milling and FDM 3D-Printing Aligning Methods. Chem. Eng. J. 402 (2020) 126218.
[9] K.A. Acord, A.D. Dupuy, U.S. Bertoli, B. Zheng, W.C. West, Q.N. Chen, A.A. Shapiro, J.M. Schoenung. Morphology, Microstructure, and Phase States in Selective Laser Sintered Lithium Ion Battery Cathodes. J. Mater. Process. Technol. 288 (2020) 116827.
[10] Y.J. Shin, R.T. Shafranek, J.H. Tsui, J. Walcott, D.H. Kim. 3D bioprinting of mechanically tuned bioinks derived from cardiac decellularized extracellular matrix. Acta Biomater. 119 (2020) 75–88.
[11] H. Wang, H. Xu, J. Zhang, S. Yu, M. Zhang. The effect of 3D-printed plastic teeth on scores in a tooth morphology course in a Chinese university. BMC Med. Educ. 20 (2020) 469.
[12] H. Zhao, C. Hong, J. Lin, X. Jin, W. Xu. Make it swing: Fabricating personalized roly-poly toys. Comput. Aided Geom. Des. 43 (2016) 226–236
[13] T. Spahiu, E. Canaj, E. Shehi. 3D printing for clothing production. J. Eng. Fibers Fabr. 15 (2020) 1–8.
[14] K. Tsai, H. Lin, Y. Chen, C. Lin, T. Hsu, C. Kao, C.K. Chua. Laser Sintered Magnesium-Calcium Silicate/Poly-"-Caprolactone Scaffold for Bone Tissue Engineering. Materials 10 (2017) 65
[15] H. Tsung-yen, D. Raj, C. Brian, T.T. Travis. 3D Printing: Current use in facial plastic and reconstructive surgery. Curr. Opin. Otolaryngol. Head Neck Surg. 25 (2017) 291–299
[16] A.P. Zwicker, J. Bloom, R. Albertson, S. Gershman. The suitability of 3D printed plastic parts for laboratory use. Am. J. Phys. 83 (2015) 281–285
[17] P.F. Costa, C. Vaquette, Q. Zhang, R.L. Reis, S. Ivanovski, D.W. Hutmacher. Advanced tissue engineering scaffold design for regeneration of the complex hierarchical periodontal structure. Clin. Periodontol. 41 (2014) 283–294
[18] J. Zuniga, D. Katsavelis, J. Peck, J. Stollberg, M. Petrykowski, A. Carson, C. Fernandez. Cyborg beast: A low-cost 3d-printed prosthetic hand for children with upper-limb differences. BMC Res. Notes 8 (2015) 10.
[19] P.F. Egan, V.C. Gonella, M. Engensperger, S.J. Ferguson, K. Shea. Computationally designed lattices with tuned properties for tissue engineering using 3D printing. PLoS ONE 12 (2017) e0182902.

[20] N. Gao, H. Hou. Sound absorption characteristic of micro-helix metamaterial by 3D printing. Theor. Appl. Mech. Lett. 8 (2018) 63–67
[21] F. Signori, M.-B. Coltelli, S. Bronco, Thermal degradation of poly(lactic acid) (PLA) and poly(butylene adipate-co-terephthalate) (PBAT) and their blends upon melt processing, Polymer Degradation and Stability 94 (2009) 74-82
[22] M. Newborough, D. Highgate, P. Vaughan, Thermal depolymerisation of scrap polymers, Applied Thermal Engineering 22 (2002) 1875-1883.
[23] A. Intisar, A. Ramzan, M. Hedar, N. Hussain, M. Bilal. Biopolymer Waste Management. In: Thomas, S., AR, A., Jose Chirayil, C., Thomas, B. (eds) Handbook of Biopolymers . Springer, Singapore, 2022.
[24] Y. Miao, A. von Jouanne, A. Yokochi. Current Technologies in Depolymerization Process and the Road Ahead. Polymers 13 (2021) 449.
[25] V. Hirschberg, D. Rodrigue, Recycling of polyamides: Processes and conditions. J. Polym. Sci. (2023) 1
[26] S.T. Phillips, A.M. DiLauro. Continuous Head-to-Tail Depolymerization: An Emerging Concept for Imparting Amplified Responses to Stimuli-Responsive Materials. ACS Macro Lett. 3 (2014) 298–304
[27] T. Ueno, E. Nakashima, K. Takeda, Quantitative analysis of random scission and chain-end scission in the thermal degradation of polyethylene, Polymer Degradation and Stability 95 (2010) 1862-1869
[28] S. S. Muobom , A.-M. S. Umar , A.-P. Brolin , Y. Soongseok. A Review on Plasticizers and Eco-Friendly Bioplasticizers: Biomass Sources and Market. INTERNATIONAL JOURNAL OF ENGINEERING RESEARCH & TECHNOLOGY 9 (2020) 1138-1144
[29] E.H. Immergut, H.F. Mark. Principles of Plasticization. in Plasticization and Plasticizer Processes Ed.: N.A.J. Platzer, Am. Chem. Soc. 1965, 1-26
[30] K. Ueberreiter, G. Kanig, Self-plasticization of polymers, Journal of Colloid Science 7 (1952) 569-583.
[31] Y. Chen, S. Zhou, S. Pan, et al. Methods for determination of plasticizer migration from polyvinyl chloride synthetic materials: a mini review. J Leather Sci Eng 4 (2022) 8.
[32] W. Zhang, N. Jiang, T. Zhang. Self-plasticization of neoprene rubber via click chemistry from environmentally sustainable cardanol. Journal of Elastomers & Plastics. 52 (2020) 483-494
[33] G.W. Scherer. Relaxation in Glass and Composites, eds. J. Wiley&Sons, New York; Wiley; 1986.
[34] I.M. Hodge. Enthalpy relaxation and recovery in amorphous materials. J Non-Cryst Sol. 169 (1994) 211-266.
[35] P.G. Debenedetti, F.H. Stillinger. Supercooled liquids and the glass transition. Nature 410 (2001) 259-267.
[36] O.A. Fridman. Structural-relaxation Mechanism of Glassy-like Polymers Plasticization. American Journal of Polymer Science 3 (2013) 7 -12.
[37] R. A. Riggleman, J. F. Douglas, J. J. de Pablo; Tuning polymer melt fragility with antiplasticizer additives. J. Chem. Phys. 126 (2007) 234903
[38] S. Araujo, N. Delpouve, A. Dhotel, S. Domenek, A. Guinault, L. Delbreilh, E. Dargent. Reducing the Gap between the Activation Energy Measured in the Liquid and the Glassy States by Adding a Plasticizer to Polylactide. ACS Omega 3 (2018) 17092–17099
[39] L. Dobircau, N. Delpouve, R. Herbinet, S. Domenek, L. Le Pluart, L. Delbreilh, V. Ducruet, E. Dargent. Molecular mobility and physical ageing of plasticized poly(lactide). Polym Eng Sci 55 (2015) 858-865.

[40] S. Valenti, L.J. del Valle, M. Romanini, M. Mitjana, J. Puiggalí, J.L. Tamarit, R. Macovez. Drug-Biopolymer Dispersions: Morphology- and Temperature-Dependent (Anti)Plasticizer Effect of the Drug and Component-Specific Johari–Goldstein Relaxations. Int. J. Mol. Sci. 23 (2022) 2456
[41] S. Araujo, N. Delpouve, S. Domenek, A. Guinault, R. Golovchak, et al.. Cooperativity Scaling and Free Volume in Plasticized Polylactide. Macromolecules 52 (2019) 6107-6115.
[42] X. Monnier, N. Delpouve, N. Basson, A. Guinault, S. Domenek, A. Saiter, P.E. Mallon, E. Dargent. Molecular dynamics in electrospun amorphous plasticized polylactide fibers. Polymer 73 (2015) 68−78
[43] E.B. Stukalin, J.F. Douglas, K.F. Freed. Plasticization and antiplasticization of polymer melts diluted by low molar mass species. J Chem Phys. 132 (2010) 084504
[44] C.A. Angell. Formation of glasses from liquids and biopolymers. Science 31 (1995) 1924-35
[45] R. Kohlrausch. Theorie des elektrischen Rückstandes in der Leidner Flasche. Annalen Physik Chem. 91 (1854) 179–213.
[46] G. Williams, D.C. Watts. Non-symmetrical dielectric relaxation behavior arising from a simple empirical decay function. Trans. Faraday Soc. 66 (1970) 80–85.
[47] J.M. Raquez, Ph. Degee, R. Narayan, Ph. Dubois, ‘‘Coordination–Insertion’’ ring-opening polymerization of 1,4-dioxan-2-one and controlled synthesis of diblock copolymers with e-caprolactone, Macromol. Rapid Commun. 21 (2000) 1063–1071.
[48] Y. Lochee, D. Jhurry, A. Bhaw-Luximon, A. Kalangos, Biodegradable poly(esterether) s: ring-opening polymerization of D, L-3-methyl-1,4-dioxan-2-one using various initiator systems, Polym. Int. 59 (2010) 1310–1318
[49] S. Nakatami, T. Matsumoto, Y. Nakahara, H. Akieda, T. Ishioyu, Purified salt of b-hydroxyethoxy acetic acid, purified 2-p-dioxanone, and manufacturing method therefore, United States Patent No. 6, 384 ,241, 2002
[50] N. Goonoo, R. Jeetah, A. Bhaw-Luximon, D. Jhurry, Polydioxanone-based bio-materials for tissue engineering and drug/gene delivery applications, Eur. J. Pharm. Biopharm. 97 B (2015) 371-391
[51] J.M. Desbordes, H. Hamard, Y. Pouliquen, Absorbable polydioxanone monofilament in the surgery of the anterior segment of the eye, J. Fr. Ophtalmol. 6 (1983) 1007–1010.
[52] J.T. Christenson, A. Kalangos, Use of a biodegradable annuloplasty ring for mitral valve repair in children, Asian Cardiovasc. Thorac. Ann. 17 (2009) 11– 12.
[53] M. Boenisch, H. Tama´ s, G.J. Nolst Trenite´ , Influence of polydioxanone foil on growing septal cartilage after surgery in an animal model: new aspects of cartilage healing and regeneration (preliminary results), Arch. Facial Plast. Surg. 5 (2003) 316–319.
[54] P.A. Madurantakam, I.A. Rodriguez, C.P. Cost, R. Viswanathan, D.G. Simpson, M.J. Beckman, P.C. Moon, G.L. Bowlin, Multiple factor interactions in biomimetic mineralization of electrospun scaffolds, Biomaterials 30 (2009) 5456–5464.
[55] S.A. Sell, M.J. McClure, C.P. Barnes, D.C. Knapp, B.H. Walpoth, D.G. Simpson, G.L. Bowlin, Electrospun polydioxanone–elastin blends: potential for bioresorbable vascular grafts, Biomed. Mater. 1 (2006) 72–80.
[56] F. Lu, X.L. Wang, S.C. Chen, K.K. Yang, Y.Z. Wang, An efficient approach to synthesize polysaccharides-graft-poly (p-dioxanone) copolymers as potential drug carriers, J. Polym. Sci. A: Polym. Chem. 47 (2009) 5344–5353.
[57] M.X. Li, R.X. Zhuo, F.Q. Qu, Study on the preparation of novel functional poly(dioxanone) and for the controlled release of protein, React. Funct. Polym. 55 (2003) 185–195

[58] R. Svoboda. Utilization of "q^+/q^- = const." DSC cycles for enthalpy relaxation studies. Eur. Polym. J. 59 (2014) 180-188.
[59] R. Svoboda. Utilization of constant heating rate DSC cycles for enthalpy relaxation studies and their influenceability by error data-distortive operations. J. Non-Cryst. Sol. 408 (2015) 115-122.
[60] Roman Svoboda, Jana Machotová, Miloš Krbal, Daniel Jezbera, Martina Nalezinková, Jan Loskot, Aleš Bezrouk, Complex thermokinetic characterization of polydioxanone for medical applications: Conditions for material processing. Polymer 277 (2023) 125978.
[61] X. Liu, S. Feng, X. Wang, J. Qi, D. Lei, Y. Li, W. Bai. Tuning the mechanical properties and degradation properties of polydioxanone isothermal annealing. Turk J Chem. 44 (2020) 1430-1444.
[62] H. Nishida, M. Yamashita, T. Endo, Y. Tokiwa. Equilibrium Polymerization Behavior of 1,4-Dioxan-2-one in Bulk. Macromolecules 33 (2000) 6982-6986
[63] H. Nishida, M. Yamashita, T. Endo. Analysis of the initial process in pyrolysis of poly(p-dioxanone). Polym. Degrad. Stabil. 78 (2002) 129 – 135.
[64] S. Arrhenius. Über die Reaktionsgeschwindigkeit bei der Inversion von Rohrzucker durch Säuren. Zeitschrift für Physikalische Chemie 4 (1889) 226-248.
[65] J. Loskot, D. Jezbera, Z.O. Zmrhalová, M. Nalezinková, D. Alferi, K. Lelkes, P. Voda, R. Andrýs, A.M. Fučíková, T. Hosszú, A. Bezrouk. A Complex In Vitro Degradation Study on Polydioxanone Biliary Stents during a Clinically Relevant Period with the Focus on Raman Spectroscopy Validation. Polymers 14 (2022) 938.
[66] J. Loskot, D. Jezbera, A. Bezrouk, R. Doležal, R. Andrýs, V. Francová, D. Miškář, A. Myslivcová Fučíková. Raman Spectroscopy as a Novel Method for the Characterization of Polydioxanone Medical Stents Biodegradation. Materials 14 (2021) 5462.
[67] M. Jaidann, J. Brisson. Conformation Study of poly(p-dioxanone) fibers by polarized raman spectroscopy, X-ray diffraction, and conformation analysis. J. Polym. Sci. Part B Polym. Phys. 46 (2008) 406–417.
[68] B. Schrader. Infrared and Raman Spectroscopy—Methods and Applications; VCH:Weinheim, Germany, 1995.
[69] A. Q. Tool. Relation between inelastic deformability and thermal expansion of glass in its annealing range. J. Am. Ceram. Soc. 29 (1946) 240.
[70] O. S. Naraynaswamy. A model of structural relaxation in glass. J. Am. Ceram. Soc. 54 (1971) 491.
[71] C. T. Moynihan, A. J. Easteal, M. A. DeBolt, J. Tucker. Dependence of the fictive temperature of glass on cooling rate. J. Am. Ceram. Soc. 59 (1976) 12.
[72] R. Svoboda, J. Málek. Description of macroscopic relaxation dynamics in glasses. J. Non-Cryst. Solids 378 (2013) 186-195.
[73] R. Svoboda. Novel equation to determine activation energy of enthalpy relaxation. J. Therm. Anal. Calorim. 121 (2015) 895-899.
[74] I. M. Hodge, A. R. Berens. Effects of annealing and prior history on enthalpy relaxation in glassy polymers. 2. Mathematical modeling. Macromolecules 15 (1982) 762-770.
[75] R. Svoboda, J. Málek. Enthalpy relaxation in Ge-Se glassy system. J. Therm. Anal. Cal. 113 (2013) 831-842
[76] R. Svoboda, D. Košťálová, M. Krbal, A. Komersová. Indomethacin: The Interplay between Structural Relaxation, Viscous Flow and Crystal Growth. Molecules 27 (2022) 5668